Journal of Colloid and Interface Science 337 (2009) 88–96

Contents lists available at ScienceDirect

Journal of Colloid and Interface Science

www.elsevier.com/locate/jcis

Lanthanide complexes on Ag nanoparticles: Designing contrast agents for magnetic resonance imaging

Talha S. Siddiqui [a], Ashish Jani [a], Florence Williams [a], Robert N. Muller [b], Luce Vander Elst [b], Sophie Laurent [b], Fang Yao [c], Youssef Zaim Wadghiri [d], Marc A. Walters [a,*]

[a] Department of Chemistry, New York University, New York, NY 10003, USA
[b] Department of General, Organic and Biomedical Chemistry, NMR and Molecular Imaging Laboratory, Université de Mons-Hainaut, Mons, Belgium
[c] School of Dentistry, New York University, New York, NY 10016, USA
[d] School of Medicine, Department of Radiology, New York University, New York, NY 10016, USA

ARTICLE INFO

Article history:
Received 8 January 2009
Accepted 29 April 2009
Available online 18 May 2009

Keywords:
MRI
Contrast
Silver
Nanoparticles
Monolayer protected
Relaxivity
Longitudinal relaxation

ABSTRACT

This paper describes colloidal particles that are designed to induce hyper-intensity contrast (T_1 relaxation) in MRI. The contrast agents consist of discrete gadolinium complexes tethered to 10 nm diameter silver nanoparticles. The gadolinium complexes (1) $[Gd(DTPA\text{-bisamido cysteine})]^{2-}$ and (2) $[Gd(cystine\text{–}NTA)_2]^{3-}$, undergo chemisorption to particle surfaces through thiol or disulfide groups, respectively, to form two new contrast agents. The resulting nanoparticulate constructs are characterized on the basis of their syntheses, composition, spectra and contrast enhancing power. The average r_1 relaxivities of the of the surface bound complexes (obtained at 9.4 T and 25 °C) are 10.7 and 9.7 s^{-1} mM^{-1}, respectively, as compared to 4.7 s^{-1} mM^{-1} for the clinical agent Magnevist™. Correspondingly, the respective whole particle relaxivities are 27927 and 13153 s^{-1} mM^{-1}.

1. Introduction

Gadolinium complexes that incorporate the ligands diethylenetriaminepentaacetic acid (DTPA) or 1,4,7,10-tetracarboxymethyl-1,4,7,10-tetraazacyclododecane (DOTA) form the radiologically active components of the magnetic resonance imaging (MRI) contrast agents Magnevist™ and Dotarem™, respectively. These agents are radiologically efficacious but non-specific in their action and are suited for the acquisition of MR images of the circulatory system (the "blood pool") and abnormalities therein [1,2]. Other common contrast agents derive from modifications of DTPA and DOTA to endow them with specificity towards certain tissues and cells [1]. In principle, high contrast and specificity are accessible with *multivalent* particles that contain surface lanthanide complexes and molecular targeting groups to augment magnetic resonance image contrast and tissue specificity [3–5]. Multivalent agents are prominent among the candidates for new targeted therapeutic agents in medicine.

The formation of thiol self-assembled monolayers (SAMS) on gold and silver nanoparticles has been applied to form colloids as well as solid phases of cross-linked particles [6–8]. Silver or gold nanoparticles accommodate homogeneous or heterogeneous sets of molecules that are covalently linked to the particle surface and are therefore ideal for the preparation of multivalent constructs. Moreover, robust attachments through physi- and chemisorption on the surface of these metals have been reported for phosphine, amine, carboxylate, thioether groups in addition to the prevalent thiol linkages [9–12]. The resulting constructs have been referred to as monolayer protected metal clusters [13,14].

The potential of noble metal colloids for diagnostics and therapeutics is glimpsed in several recent reports [15–21]. In this paper we focus on surface coordination complexes for which a silver metal core is the supporting structure. The aim of this research is to optimize the formation and analysis of noble metal based imaging agents and to evaluate the analytical tools required for their production. The constructs discussed below aid in the assembly of tools for the development of multivalent nanoscale MRI contrast agents. They consist of NTA and DTPA diamide ligands with pendant thiol groups for binding to silver nanoparticle surfaces. The DTPA diamides are chemically related to those described in earlier studies of oligomeric GdDTPA complexes linked by disulfide bonds [22,23].

2. Materials and methods

All chemicals were used as received. Carbon-13 and proton NMR data sets were obtained on a Bruker Avance 400 MHz NMR spectrometer. Thermogravimetric analyses (TGA) were carried out on a

* Corresponding author. Address: NYU Dept. of Chemistry, 100 Washington Square E., New York, NY 10003, USA. Fax: +1 212 260 7905.
E-mail address: marc.walters@nyu.edu (M.A. Walters).

0021-9797/$ - see front matter © 2009 Elsevier Inc. All rights reserved.
doi:10.1016/j.jcis.2009.04.096

Texas Instruments SDT Q600 and a Perkin-Elmer Pyris 1. TGA profiles were recorded by using a Universal Analysis program. Electrospray ionization mass spectrometric data were obtained using an Agilent 1100 Series Capillary LCMSD Trap XCT MS spectrometer. Infrared data were obtained on a Nicolet 750 spectrometer. TEM images were acquired from samples on carbon coated copper grids examined under a Philips CM-12 electron microscope. The micrographs were recorded on a Gatan 1 k × 1 k digital camera. For nuclear magnetic resonance dispersion measurements between 0.01 and 10 MHz, the relaxation rates were measured on a Stelar relaxometer, and at 20 MHz on a Minispec Bruker mq-20. Samples were contained in 10 mm o.d. pyrex tubes. Measurements at 60 MHz were performed using tubes of 7.5 mm o.d. Measurements at 500 MHz on a Bruker Avance II spectrometer were carried out for samples of less than 25 μl, contained in capillary tubes. Deionized water was used to prepare samples for NMR measurements.

For relaxivity measurements samples were stabilized at 25 °C with a variable temperature unit BVT-3200. Acquisition parameters were: time domain 16 K complex data point; 6410.26 Hz sweep width; 90° pulse with a length of 9 μs, at a power level of 5.00 dB repetition time T_R of 45 s; variable inversion time delay (τ) ranging from 100 ms to 5 s. Spectra were processed with XWIN-NMR version 3.5.6 to obtain relaxation curves.

For the acquisition of MRI phantom data the samples were contained in Kimble borosilicate glass tubes 6 mm o.d. × 50 mm length. The MR images were acquired at 3 Tesla using a T_1-weighted 2D Gradient sequence (repetition time TR = 22 ms, echo time TE = 9 ms, flip angle FA = 90°).

3. Synthesis of DTPA-L-cys (2)

L-Cysteine 1.76 g (11.19 mmol) was deprotonated in 100 ml water with Na_2CO_3 0.59 g (5.59 mmol). To this solution, DTPA-bis-anhydride (**1**) [24], 2.0 g (5.59 mmol) was added, and the solution was stirred at room temperature for 24 h. The crude product was dried, redissolved in methanol, and filtered to remove by-product salts. The solvent was removed under vacuum and the product was washed with acetone and then dried under vacuum leaving a yellow powder. Yield 93%.

ESI-MS: H_2O with anion detection
$[M\text{-}H]^-$ 598 *m/z*; $[M - nH + (n-1)Na]^-$; 620.1 *m/z* ($n = 1$), 642.1 *m/z* ($n = 2$), 664.1 *m/z* ($n = 2$).
IR (KBr pellet):
3422.55 cm^{-1}(-OH), 1601.65 cm^{-1}(CO), 1400.45 (-NHCO) cm^{-1}.

4. Synthesis of [Gd(DTPA-L-cys)] (3)

Compound **2**, 0.25 g (0.418 mmol) was dissolved in 30 mL of water following which Gd_2O_3 75.8 mg (0.209 mmol) was added with stirring. The resulting suspension was refluxed for 4 h. Water was removed under vacuum and the resulting solid was washed with acetone collected by vacuum filtration and dried under vacuum, 82% yield [25].

ESI-MS: in H_2O with anion detection
$[M\text{-}H]^-$ 754 *m/z*

5. Preparation of DTPA-cys derivatized silver nanoparticles (5–7)

Silver nanoparticles were prepared by the method of Kim et al. [26] An aqueous 1 mM stock solution of silver nitrate, $AgNO_3$, 10 mL (0.01 mmol), was added with stirring to 30 mL of aqueous 2 mM $NaBH_4$, (0.06 mmol) on an ice bath. The resulting yellow–brown light-sensitive solution was handled in a light shielding reaction vessel. Thiol-containing molecules (0.01 mmol) were added to this solution either in ligand form **2** or as lanthanide complexes **3,** and [La(DTPA-L-cys)] (**4**), to obtain, DTPA-L-cys{Ag} (**5**), [Gd(DTPA-L-cys)]{Ag} (**6**), and [La(DTPA-L-cys)]{Ag} (**7**), where surface derivatized Ag nanoparticles are denoted by the symbol {Ag}. The solution was stirred for 30 min, concentrated to approximately 5.0 mL by rotary evaporation followed by dialysis (membrane:1200 MW cutoff) against distilled water overnight.

6. Synthesis of cystine-*N,N′*-tetraacetic acid (cystine–NTA; K_4H_2CNTA) (8)

A solution of potassium bromoacetate was prepared from 12.68 mL of aqueous KOH (6.4 M) and 11.28 g of bromoacetic acid (81.15 mmol) and added to L-cystine 3.00 g (12.48 mmol) in 3.9 mL of aqueous KOH (6.4 M). An additional 12.68 mL of KOH (aq) (6.4 M) was then added to the reaction solution following which the reaction flask was left unstirred for three days. The solution was diluted with 350 mL of methanol and allowed to stand overnight. Deposited solids were collected by filtration and the product was washed free of salts by Soxhlet extraction in methanol for 24 h leaving the product which was collected from the Soxhlet thimble and dried under vacuum to give 3.99 g of $K_3H_3CNTA{\cdot}4\,H_2O$, 49% yield.

ESI-MS in H_2O with anion detection

$[M\text{-}H]^-$ 471.1 *m/z*. Peaks at 509.0 *m/z*, 547.0 *m/z*, and 584.9 *m/z* correspond to $[KH_4CNTA]^-$, $[K_2H_3CNTA]^-$, and $[K_3H_2CNTA]^-$, respectively.

Elemental analysis: C 24.36, H 3.09, N 3.76, K 17.99% corresponding to $K_3H_3CNTA{\cdot}4H_2O$, expected: C 25.52, H 3.83, N 4.25, K 17.8%.

7. Synthesis of cystine-*N,N′*-tetraacetic acid on Ag, (CNTA{Ag}) (9)

The compound Ag-cystine-*N,N′*-tetraacetic acid, (CNTA){Ag} (**9**), was prepared from compound **8** and an Ag sol as above for compound **5**.

8. Preparation of $[La(CNTA)_2]${Ag} (10) for ^1H and ^{13}C NMR

Compound **8**, $K_3H_3CNTA{\cdot}4H_2O$, 6.58 mg (0.01 mmol) was added to Ag nanoparticles in 40 mL of water, prepared as above. Lanthanum trichloride, $LaCl_3{\cdot}7H_2O$ (2.45 mg, 0.01 mmol), was then added and the solution was stirred overnight. The resulting clear light brown solution was concentrated to a volume of approximately 5 mL by rotary evaporation and was then dialyzed against distilled water overnight. The sample was then dried under vacuum and the resulting dark solid was dissolved in 0.5 mL of D_2O for NMR analyses. The synthesis of $[Gd(CNTA)_2]${AG} is described in Supporting information.

9. Results and discussion

9.1. Syntheses

9.1.1. DTPA-L-cys

Diethylenetriamine pentaacetic acid (DTPA) is the foundation for numerous ligands that bind Gd^{3+} in the formation of MRI contrast agents. The well known α,ω-bisamide derivatives of DTPA can be formed from primary amines to introduce pendant groups for targeting moieties, attachment sites, chelators and the like. We formed a bis-amide of DTPA that contains thiols for the attachment of ligand–lanthanide complexes to silver nanoparticles.

Recently, Debouttière et al. [19] showed that bis 1,7-(*N*-cystamine acetamido)diethylenetriamine-1,4,7-triacetic acid forms a

complex with gadolinium and binds to gold nanoparticles. The resulting complex was employed as an MRI contrast agent and was reported to have a relaxivity of 3.9 $Mm^{-1}\,s^{-1}$ per Gd ion at 7 T, and presumably under ambient (25 °C) conditions. Independently, we synthesized the same complex and found its water solubility to be low. However, when cysteine was employed instead of cystamine the free additional carboxylate groups enhanced the solubility of the complex (compound **3**). The resulting ligand, DTPA-L-cys (**2**) (Fig. 1), was formed through the reaction of the 1,7-bisanhydride of DTPA with two equivalents of cysteine in water [24]. Standard workup procedures gave the product in high yield. The ligand was then combined with lanthanide ion to form an isolable complex. Silver bound lanthanide complexes of DTPA-L-cys were then formed by the simple addition of the complexes to colloidal silver in aqueous solution.

Whereas we employed cysteine carboxylate groups to enhance the solubilities of our nanoparticles Alric et al. [20] took the approach by leaving a subset of DTPA groups uncoordinated to allow water to solvate free carboxylate groups along a chain of oligomeric DTPA ligands. The reported result was a significant enhancement in the solubility for $[GdDTPA\text{-}cystamine]_n\{Au\}$ contrast agent. While these two approaches exploit free carboxylates to increase the solubilities of the respective particles one concern is that uncomplexed DTPA, employed by Alric et al. might scavenge endogenous metal ions from serum and tissue with undesirable consequences. The synthesis of this class of DTPA derived nanoparticle is, never the less, an important exploration of multivalent diagnostic agents. In a recent publication we note the confirmatory results of Park, and coworkers who, employed glutathione which like the one described in this paper, bears carboxylates that aid solvation [21].

Nephrogenic systemic fibrosis (NSF) is a condition that is linked to the release of Gd^{3+} ions from contrast agents when clearance is slow in adults as a result of kidney damage and in infants as a result of low capacity. The risk of NSF is particularly great when the Gd^{3+} binding stability constant is low in a particular contrast agent. Accordingly, it is of interest to know the stability constants for agents that incorporate GdDTPA sites. Such measurements have been made for *molecular* contrast agents [27]. The standard approach involves the determination of a conditional stability constant at low pH in order to induce equilibration of Gd with the coordinating indicator dye, arsenazo. Under these conditions the silver nanoparticulate construct is not expected to be stable. However the stability constants for GdDTPA diamides are known to be a function of the number of carboxylates available for Gd^{3+} binding. It is reasonable to expect the DTPA-cys{Ag} to have a thermodynamic stability constant $\log K \approx 16$ [27]. The data acquired with this construct should be interpreted on this basis.

9.1.2. Cystine–NTA

Bis–NTA complexes of gadolinium have been reported in which tetracoordinate NTA provides a net eight coordination of the gadolinium ion [28–30]. We therefore expected cystine–NTA (CNTA) to form an eight coordinate complex with gadolinium. Cystine–NTA was prepared by the reaction between cystine and excess bromoacetic acid in a basic aqueous solution. The synthesis of cystine-*N*,*N*′-tetraacetic acid (**8**) was based on an earlier preparation by Michaelis and Schubert [31]. Product formation was optimal for reactants in the ratio of KOH:bromoacetic acid:cystine 6.5:6.5:1. The crude product was precipitated from methanol/water and then purified by washing with methanol in a Soxhlet extractor. The isolated form of the product differs from the expected stoichiometry of K_4CNTA. Elemental analysis showed the product to be $K_{3.5}H_{2.5}CNTA$, consistent with a mixture of K_3HCNTA and K_4CNTA. For simplicity we refer to the mixture as K_4CNTA in this discussion.

Potassium CNTA formed a Ln^{3+} complex, $[Ln(CNTA)_2]^{3-}$, that was weakly soluble in water, in stark contrast to $[Ln(NTA)_2]^{3-}$ which is freely soluble. The low solubility of $[Ln(CNTA)_2]^{3-}$ suggests that the complex is oligomeric. In the assembly of $[Ln(CNTA)_2]^{3-}$complex on Ag, K_4CNTA was mixed with Ag nanoparticles prior to the introduction of Ln^{3+}. This sequence of addition avoided an oligomerization process that would likely impede the assembly of complexes on the particle surface.

In spite of its tetracoordinating capacity, a single NTA ligand is predicted to form a relatively weak complex with lanthanides [32]. By contrast, bis–NTA complexes of lanthanides are more stable by several orders of magnitude. The probability of bis–NTA ligation is increased by the enforced proximity of NTA groups that are tethered to the particle surface through stable covalent bonds. Further, the lanthanide–NTA complex stability constant should be very high for complexes formed by NTA in this environment as predicted by the *surface chelate effect* [33]. A simple explanation of this effect is that the two halves of the ligand are bridged by a small region of the metal particle surface thereby forming an enhanced chelating structure. The details of ligand uptake by Ag particles were elucidated by ^1H NMR data as described below. Because of the aforementioned instability of Ag colloids we did not attempt to determine the stability constants for this construct.

9.2. NMR of DTPA-L-cys, Ag and Ln^{3+} binding

Debouttière et al. [19] and later Alric et al. [20] describe having functionalized gold nanoparticles with a DTPA-bis(mercaptoethylamide) derivative to obtain a construct in which the oligomerized ligand is thought to form looped structures on the particle surface. In an effort to form constructs with a layer of *monomeric* dithiol compounds on the silver surface we prepared the bare silver particles and only afterwards added ligand in the presence of $NaBH_4$, to minimize disulfide formation. The solutions containing DTPA-L-cys{Ag} were then dialyzed to remove free ligand. NMR data showed that the DTPA bis-amide complex of La^{3+} binds to the silver particle surface. However, because of peak broadening, the data was not illuminating with regard to the presence of oligomers.

Proton and ^{13}C NMR data were acquired on DTPA-L-cys(**2**), [La(DTPA-L-cys)] (**4**), and [La(DTPA-L-cys)]{Ag}(**7**) (Figs. 2 and 3). Proton and carbon NMR resonance assignments were verified from one-bond C–H (HSQC) and multiple-bond H–C–C (HMBC) coupling crosspeaks (Fig. 3). The unique coupling pathway starts at the H-6 proton (3.75 ppm) and gives a crosspeak that shows coupling to C-6 (55 ppm). The three-bond coupling of H-6 to C-4 (52 ppm) is clear in the HMBC contour plot. Likewise the coupling of H-4 to C-3 (50 ppm) appears in the HMBC spectrum. The remaining assignments were similarly derived.

In a series of NMR studies [34–36] Peters and coworkers showed that the tricapped trigonal prismatic structure of the

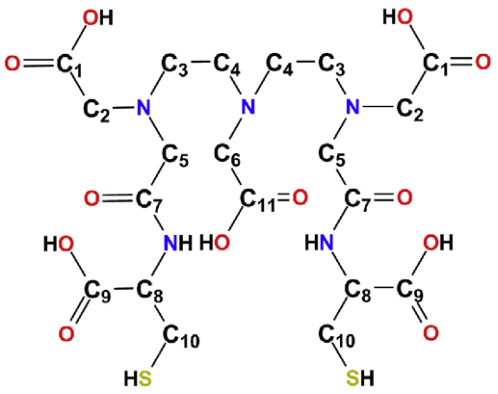

Fig. 1. DTPA-L-cys, (**2**) neutral form.

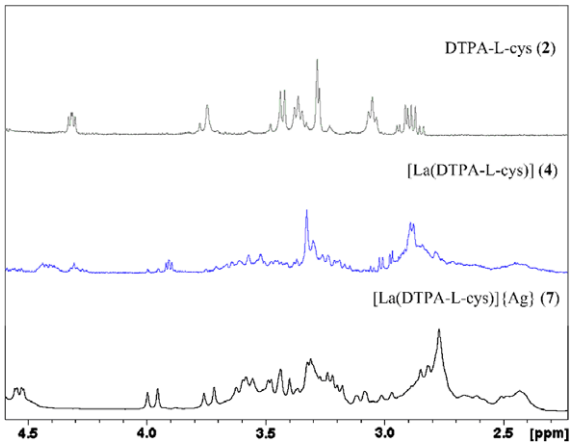

Fig. 2. ^{1}H NMR at 400 MHz of DTPA-L-cys (**2**), [La(DTPA-L-cys)] (**4**), and [La(DTPA-L-cys)]{Ag} (**7**) in D_2O. Samples were 1 ml in volume and contained 2.5×10^{14} particles.

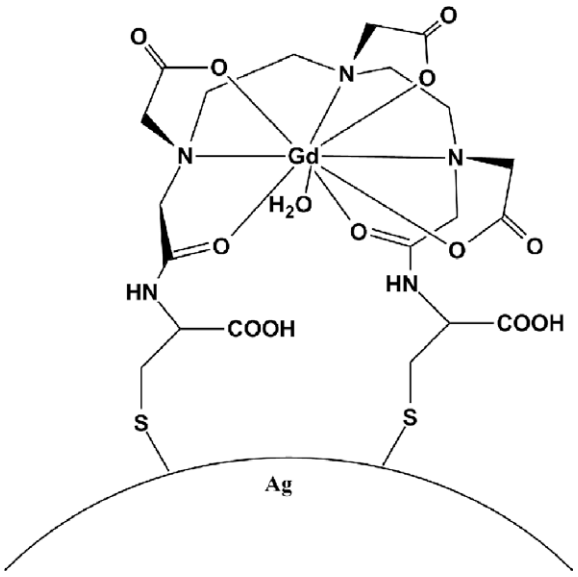

Fig. 3. [La(DTPA-L-cys)]{Ag} (**6**).

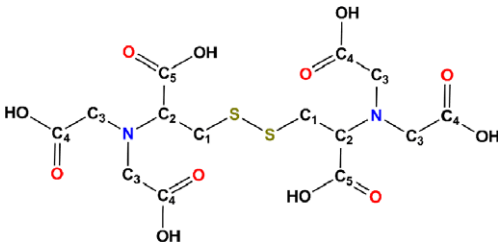

Fig. 4. CNTA, (**8**) neutral form.

diamagnetic complex LaDTPA is chiral. In the solution phase the compound furthermore interconverts between eight enantiomeric and four diastereomers structures. The α,ω-bisamide derivative of DTPA-L-cys (**2**) has two additional chiral centers, which increases the number of stereoisomers by a factor of four [36]. At ambient temperature a mix of stereoisomers produces inhomogeneously broadended NMR peaks [37]. In an NOESY study of a La^{3+} complex of triethylenetetraaminehexaacetic acid (TTHA), Lee et al. found that at ambient temperature the metal ion undergoes dynamic re-coordination steps in the solution phase that generates a complex NMR pattern [38]. However, at elevated temperature where the fast exchange limit is reached, nine distinct peaks appear for the acetate and methylene groups [39]. It is probable that the complex room temperature spectrum of [La(DTPA-L-cys)] (**4**) is due to an intermediate rate of carboxylate exchange (Supporting information). The two carboxylate groups of cysteine in **2** are potential coordination sites for La^{3+} that might further contribute to exchange broadening. The chemisorption of [La(DTPA-L-cys)] (**4**) on Ag nanoparticles to form [La(DTPA-L-cys)]{Ag} (**7**) is similarly marked by significant peak broadening and a complex ^{1}H NMR pattern (Figs. 4 and 5).

Lanthanum coordination by DTPA-L-cys (**2**) was monitored by ^{13}C NMR spectra (Supporting information). The appearance of multiple carbonyl peaks in the 174–192 ppm range is a consequence of fluxional stereoisomerization [34–37,39]. Downfield shifts of both the carbonyl and aliphatic carbon peaks of the ligand, **2**, accompany the formation of the lanthanum complex, **4**, which is congruent with an earlier study by Choppin et al. of $[La(DTPA)]^{2-}$ [40]. Several of the peaks were broadened by conformational fluctuations. Peaks due to the aliphatic carbons C8 and C10 shifted slightly upfield as confirmed by an HSQC spectrum. The ^{13}C NMR data (Supporting information) show cysteine to remain uncoordinated

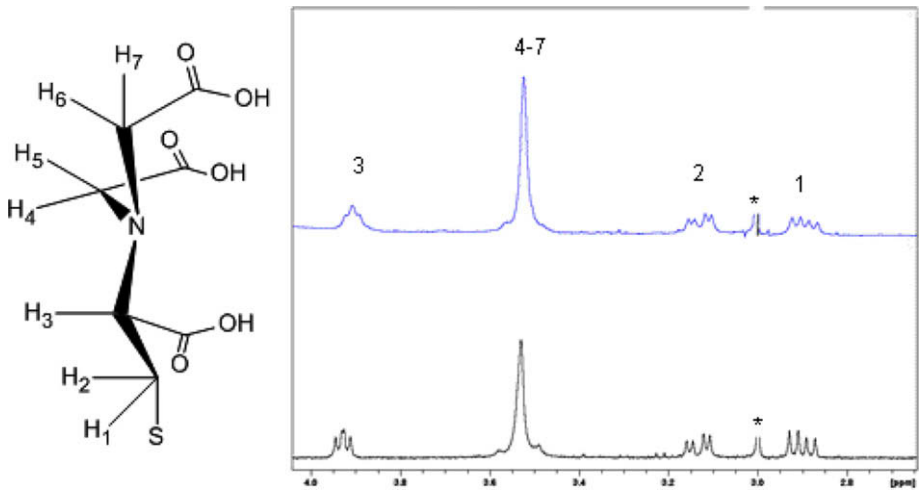

Fig. 5. ^{1}H NMR at 400 MHz of CNTA (**8**), bottom, and CNTA{Ag} (**9**) top in D_2O. Particle concentrations were the same as reported for Fig. 2. (* MeOH impurity).

in the lanthanum complex [La(DTPA-L-cys)] (**4**), leaving the carboxylate and thiolate groups free.

Further broadening of the ligand ^{13}C peaks accompany the binding of **4** to the Ag surface to form [La(DTPA-L-cys)]{Ag}. The peaks for C8 (56 ppm) and C10 (25 ppm) of cysteine disappear, probably as a result of broadening (Supporting information). Similar extreme broadening was reported by Murray and coworkers who found that carbon peaks of alkane capped gold nanoparticles where broadened by proximity with the gold surface. The peak for the carbon atom next to the sulfur was broadened into the baseline. The effect of metal surface proximity on peak broadening may be due to a Knight effect or to the paramagnetism of an odd electron metal core [41].

9.3. CNTA ^{13}C and ^{1}H NMR

The uptake and orientation of K_4CNTA (Fig. 4) and its lanthanum complex on silver nanoparticles were determined from ^{1}H NMR data (Fig. 5). Overall, the ^{1}H NMR peaks of the bound ligand in the construct, [K_4CNTA)]{Ag}, (**9**) were slightly broadened but otherwise fully congruent with the peaks of the free ligand. The relative uniformity of the broadening was surprising since it did not exhibit the expected dependence on distance of the proton from the silver surface [41].

Data from ^{13}C NMR revealed a diminution of the carbonyl peaks for **9**, likely due to peak broadening, which would be consistent with carboxylate group binding to the silver particle surface. It is noteworthy that the signal for the C1 carbon remains sharp, which suggests that the attachment of CNTA to the silver particle surface does not involve sulfur. The disulfide bond remains intact and is sterically shielded from the Ag particle surface (Fig. 6). Evidence for preferred binding of carboxylate in disulfide-containing molecules has been presented in recent literature on the surface enhanced Raman spectra of cysteine and cystine on silver and gold surfaces [42,43].

Several new peaks were observed in the ^{1}H NMR spectrum of the lanthanum complex (**10**) bound to silver. We believe this to result from an asymmetry of the H4 hydrogen atoms (Supporting information) that occurs upon complex formation. This interpretation is supported by the work of Lee et al. who reported a doubling of triethylenetetraamine hexaacetic acid ^{1}H NMR resonances upon uptake of lanthanum ion [38]. In complex **10** a subset of the proton resonances observed in the free ligand doubled upon lanthanum complex formation. Peak assignments are based on HSQC data. The appearance of well defined NMR resonances for complex **10** suggests that the complex is at the fast exchange limit for NMR. In analogy with the La DTPA complex it is likely that the slow exchange limit is accessed only at very low temperature.

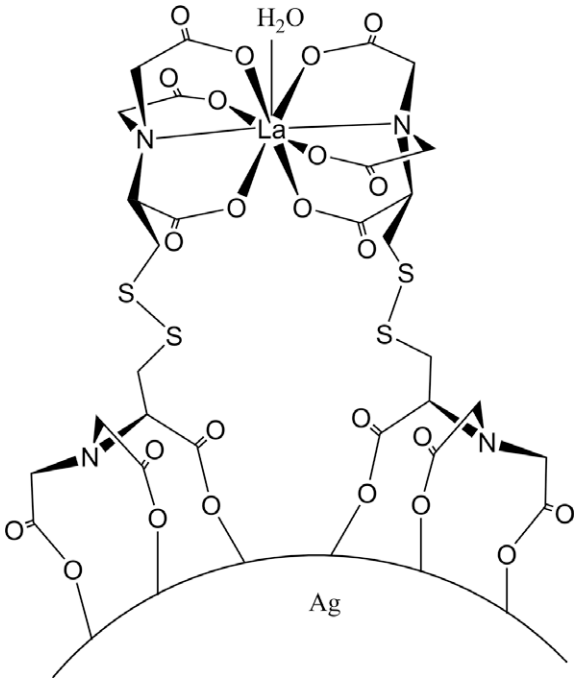

Fig. 6. [La(CNTA)$_2$]{Ag} (**10**).

9.4. UV–visible Spectra

Bare silver nanoparticles of 10 nm diameter have been reported to have a surface plasmon resonance peak ca. 400 nm [26,44,45]. Our bare Ag nanoparticles have an absorption peak at 389 nm (Table 1). A red shift is observed in the 389 nm feature for surface functionalized Ag nanoparticles with DTPA-L-cys compounds (**5**) and (**6**) chemisorb to the particle surface and generate red shifted resonances at 395 and 408 nm, respectively. These red shifts are in accord with earlier reports [46,47]. In the second set of compounds, the CNTA derivative on silver (**9**), and the Gd bound CNTA derivative on silver (**11**), a similar red shift occurred, with new peaks arising at 406 and 414 nm, respectively.

9.5. Transmission electron microscopy (TEM)

TEM images were obtained for DTPA-L-cys{Ag} (**5**) and [Gd(DTPA-L-cys)]{Ag} (**6**). Particle aggregation occurred to varying extents in two of the samples as has been previously observed in silver nanoparticles [48]. In general, individual particles were observed under TEM to have an average size of 10 nm (Fig. 7). In the TEM images of the CNTA{Ag} constructs **9** and **11** particle aggregation was similarly observed (Fig. 8).

9.6. Thermogravimetric analysis (TGA)

Samples of GdDTPA-L-cys{Ag} (**6**), and GdCNTA{Ag} (**7**) were isolated by lyophilization to yield air stable brown/black powders for TGA analysis. The TGA data for [GdDTPA-L-cys]{Ag} (**6**) shows a downward slope corresponding to a 20% mass loss in the temperature range below 300 °C (Fig. 9a). The mass loss in this region is generally attributed to the dissociation of bound water such as described in a study by Aukrust et al. on the lanthanide complex GdDTPA bis(methylamide) [49]. Following the dissociation of water, these workers observed the onset of decomposition of the complex in the 300–320 °C region. Similarly, in the study of nanoparticles, thiol dissociation/decomposition on silver has been observed to begin in the vicinity of 300 °C [50,51], but in the case of benzylthiol occurs as low as 200 °C [52]. In the latter case the thiol was conjectured to dissociate as a volatile disulfide[52,53], which would not be expected for a DTPA complex.

For the compound [Gd(DTPA-L-cys)]{Ag} (**6**), mass loss in the region below 300 °C likely corresponds to both weakly and strongly bound water [49,51]. The strongly bound water fraction might be covalently bound to Gd^{3+} ions. The loss of 26% of the mass in the temperature range 300–400 °C can be attributed to the decomposition of the organic component of the construct. From this analysis we found 2610 complexes per Ag particle (Table 2). The corresponding footprint of complexes on the 10 nm particle surface would be approximately 12 Å^2/complex, which is relatively small and suggests that some complexes remain unbound forming a looped oligomeric structure above the metal surface [54,55].

For the complex [Gd(CNTA)$_2$]{Ag} (**11**) the TGA profile was quite similar to that of complex **6** (Fig. 9b). Mass loss below 300 °C, is assigned to water. In the 300–400 °C range there is a mass decrease of 23% that is assigned to the organic component of the construct.

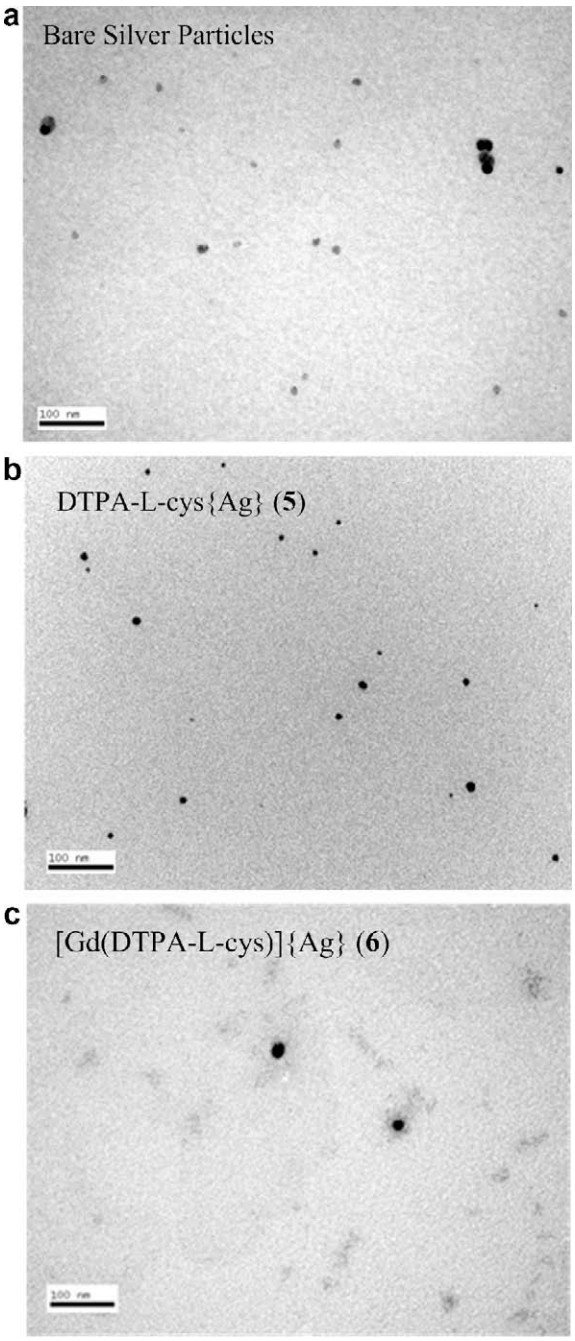

Fig. 7. TEM images silver particles (top), DTPA-L-cys{Ag} **5** (middle), and [Gd(DTPA-L-cys)]{Ag} **6** (bottom).

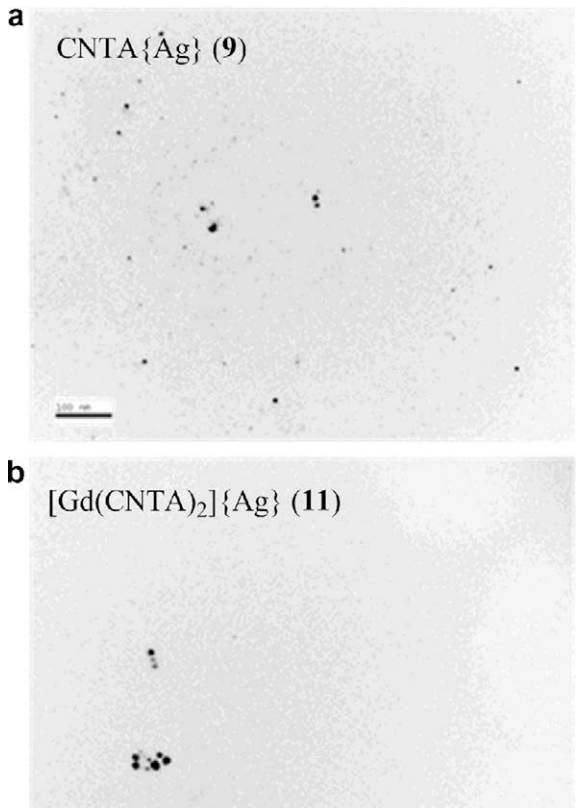

Fig. 8. TEM images CNTA{Ag} (**9**) (top) and [Gd(CNTA)$_2$]{Ag} (**11**) (bottom).

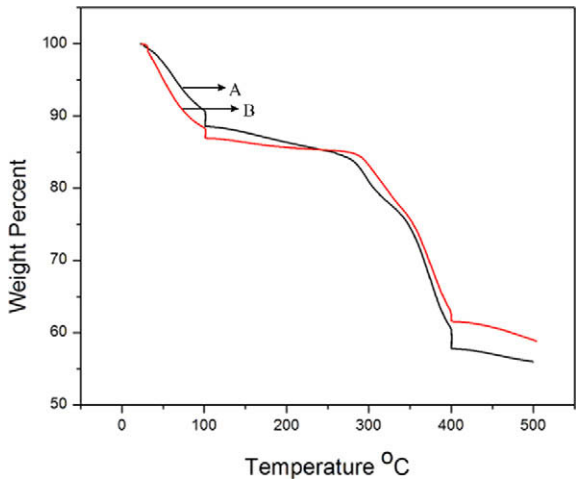

Fig. 9. Thermograms for (A) [GdDTPA-L-cys]{Ag} (**6**) and (B) [Gd(CNTA)$_2$]{Ag} (**11**). The organic mass is 26% of the sample mass of (A) and 23% of (B).

The number of complexes that are surface bound for **11** is 1356 (Table 2). The corresponding footprint of this complex is 23 Å^2/complex, which would be consistent with all of the complexes being surface bound.

The number of silver particles per sample was required for the determination of the number of complexes per particle. The former was calculated from the mass of the white powder silver nanoparticles that remained after TGA pyrolysis, each with an average 10 nm diameter and a density of 9.0 g/cm^3 [56,57].

Table 1
UV–vis absorbance peaks.

Compound	Absorbance (nm)
Bare Ag nanoparticles	389
DTPA-L-cys{Ag} **5**	395
[Gd(DTPA-L-cys)]{Ag} **6**	408
CNTA{Ag} **9**	406
[Gd(CNTA)$_2$]{Ag} **11**	414

9.7. r_1 Relaxivity studies

Data were collected on Gd complexes in aqueous solutions each contained in the outer compartment of a 5 mm coaxial tube with an inner tube containing pure D_2O to provide a lock frequency. Relaxivity measurements on complexes were also acquired (at

Table 2
Relaxivity (r_1) per Gd (except where noted) in H_2O (except where indicated) at 9.4 T (400 MHz), 25° C.

Compound	Complexes per particle	Relaxivity (s^{-1} mM^{-1})
$[Gd(DTPA)]^{2-}$		4.6 5.2 (in D_2O)
[Gd(DTPA-L-cys)]{Ag} (**6**)		10.7
$[Gd(CNTA)_2]${Ag} (**11**)		9.7
[Gd(DTPA-L-cys)]{Ag} (**6**)	2610	27927[a]
$[Gd(CNTA)_2]${Ag} (**11**)	1356	13153[a]

[a] Relaxivity per particle is estimated from the Gd^{3+} population of the particle surface.

400 MHz) on samples in D_2O solution in simple 5 mm NMR tubes. For the latter experiments, the residual water in D_2O provided the signal necessary to determine the proton relaxation rate in the medium. Longitudinal relaxivity (T_1) values were determined using the standard inversion recovery pulse sequence 180° – τ[variable delay] – 90° – acquire. Relaxivity values r_1 were determined by calculating the slope of a graph of $R_1(1/T_1)$ vs. Gd concentration (Eq. (1)):

$$(1/T_1)_{obs} = (1/T_1)_d + r_1[Gd] \quad (1)$$

where $(1/T_1)_{obs}$ is the relaxation rate in presence of contrast agent and $(1\backslash T_1)_d$ is the relaxation rate in the absence of contrast agent. No aggregation was observed prior to or after the course of data collection.

For all compounds the r_1 values reported were *per Gd*$^{+3}$ ion, and, where indicated, *per particle* for nanoparticulate constructs (Table 2). Values for r_1 (acquired at 400 MHz) in the range of 5–6 s^{-1} mM^{-1} $[GdDTPA]^{2-}$ are in agreement with published data acquired at 400 MHz [58–61]. Compound **3**, [Gd(DTPA-L-cys)], exhibits a relatively high relaxivity of 9.2 s^{-1} mM^{-1} in D_2O (25 °C), that might be explained by the oligomerization of the complexes by disulfide bond formation. In contrast, GdDTPA has a relaxivity of 4.6 s^{-1} mM^{-1} in H_2O and 5.2 s^{-1} mM^{-1} in D_2O. The effect of D_2O on the value of r_1, which may result from differences in viscosity (D_2O, 1.100 cP; H_2O, 0.8903 cP at 25 ° C) [62] and exchange rate deserves further investigation. Oligomerization of compound **3** might be expected to increase the rotational correlation time of the complexes and the resultant contribution of τ_r to the T_1. Oligomerization of this type has been reported by Debouttière et al. and Alric et al. [19,20] for ligands whose structures are closely related to DTPA-L-cys.

The r_1 values for [Gd(DTPA-L-cys)]{Ag} (**6**) and $[Gd(CNTA)_2]${Ag} (**11**) are 10.7 and 9.7 s^{-1} mM^{-1} (per Gd^{3+} ion), respectively. These values are approximately two times greater than the r_1 value of 4.6 s^{-1} mM^{-1} for $[Gd(DTPA)]^{2-}$ in aqueous solution. The most plausible explanation for the high values is an increase in the rotational correlation time, τ_R, of the nanoparticles which should increase relaxivities in nanoscale contrast agents [63,64].

9.7.1. MRI phantoms

MRI phantoms were obtained from aqueous solutions of Magnevist and construct **6** (Fig. 10). The degree of brightening of the contrast agent was determined from the signal-to-noise ratio (SNR). The SNR was measured as mean signal intensity of a region within the sample tube divided by the standard deviation of the background signal from air. The water standard (bottom tube) gave a SNR value of 16. A 1.0 mM aqueous solution of the complex GdDTPA had a value of SNR = 65 which increases to a value of 88 when tethered to silver nanoparticles (top tube).

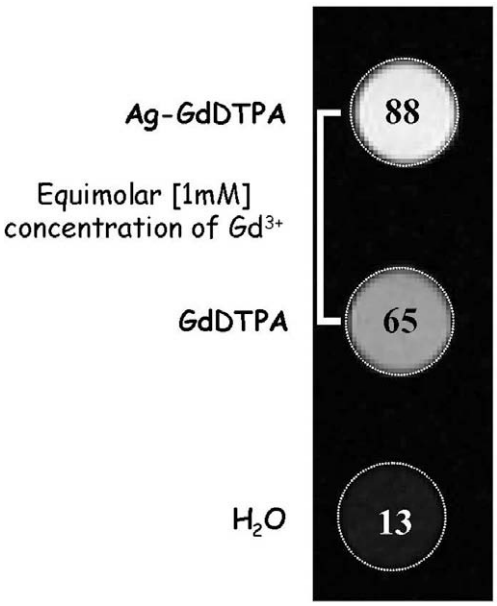

Fig. 10. MRI phantoms of [GdDTPA-L-cys]{Ag} (**6**) (1.0 mM) (top), Magnevist (aq) (1.0 mM) (middle), and water (bottom).

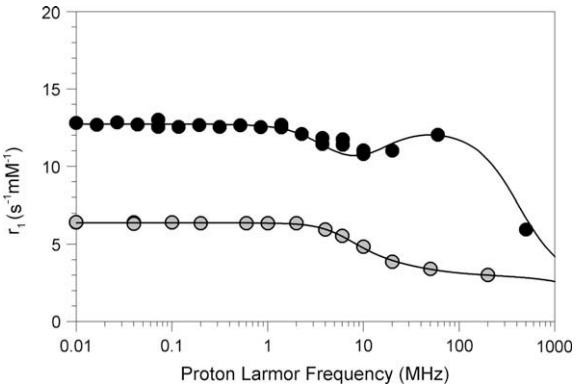

Fig. 11. NMRD of GdDTPA (2.0 mM, 37 °C) (grey circles) and [Gd(DTPA-L-cys)]{Ag} (2.75 mM, 37 °C) (**6**) (black circles). The lines through the data correspond to the theoretical fitting; for Gd-DTPA see Ref. [67]; for [Gd(DTPA-L-cys)]{Ag} the following parameters were used: τ_{SO} = 84 ps, τ_V = 27 ps, τ_M = 1 μs, q = 1, r = 0.31 nm, τ_R = 0.55 ns, τ_{SS} = 40 ps, q_{ss} = 4, r_{ss} = 0.36 nm, $D = 3 \times 10^{-9}$ m textsuperscript2 s^{-1}, d = 0.4 nm.

9.7.2. Nuclear magnetic resonance dispersion (NMRD) measurements

An NMRD profile for construct [Gd(DTPA-L-cys)]{Ag} (**6**) is shown in Fig. 11. The measurements were performed at 37 °C within 2 h of sample solution preparation. No change in the homogeneity of the sample was noticed during the measurements. The measurements at 500 MHz were performed during the next hour. Due to the limited solubility of this class of nanoparticle, some aggregation was observed after 3–4 h.

The per-Gd^{3+} relaxivity values are significantly higher than those of GdDTPA at all magnetic field strengths and are typical of a slowly rotating system as indicated by the "hump" around 60 MHz. A theoretical adjustment of the experimental data with a model including outersphere, innersphere and second sphere contributions was performed. The results shown in Fig. 11 agree with a global rotational correlation time of about 0.55 ns and the presence of four water molecules in the second sphere. From the NMRD data we see that at the clinical field of 1.5 T (64 MHz) the relaxivity of [Gd(DTPA-L-cys)]{Ag} (**6**) per gadolinium is approxi-

mately 11 s^{-1} mM^{-1}. Similarly, at 9.4 T (400 MHz) the relaxivity for this compound is 10.7 s^{-1} mM^{-1} (Table 2). The multiplicative effect in construct **6** would produce a contrast agent with a relaxivity of 28710 s^{-1} mM^{-1}. Further, the local concentration of Gd^{3+} is 8.29 M based on a particle radius of 5 nm, and a surface loading of 2610 complexes per particle.

10. Conclusions

Silver particles were functionalized by the chemisorption of a series of lanthanide complexes. The constructs were examined by NMR and UV–vis spectroscopy to verify the surface derivatization of the particles. TEM and TGA were used to determine the number of complexes bound to the particle surface. Relaxivity, r_1, was determined for the particles with results that were greater than that of the FDA approved contrast agent Magnevist® when computed on a per Gd ion basis. The nanoparticulate constructs reported here can be modified to include targeting moieties for cell labelling or for the detection of lesions that are accessible from the circulatory system. We propose that the constructs similar to those described above, but carefully selected to exhibit high stability constants, would be well suited as multivalent, high payload contrast agents. Their relaxivities are among the highest that have been reported for a T_1 contrast agent.

The ideal nanoparticulate contrast agent would consist of a multifunctional construct that can be cleared from the body, preferably through the renal system, within hours of initial administration. Quantum dots composed of CdSe-ZnS and in the size regime $\leqslant$5.5 nm diameter were found to satisfy that clearance criteria [65,66]. While the particles reported here do not fit this criterion their preparation in this size regime can be easily realized for biological applications.

Acknowledgments

This work was supported in part by a grant from the Tilker Medical Research Foundation (Y.Z.W. and M.A.W.). We wish to thank Dr. Alice Liang for the acquisition of electron micrographs. We thank Dr. Chin Lin for assistance in the NMR analyses. This work was supported by the FNRS and the ARC Program 05/10-335 of the French Community of Belgium. The support and sponsorship concerted by COST Action D38 and the EMIL project are kindly acknowledged (R.M.).

Appendix A. Supplementary data

Supplementary data associated with this article can be found, in the online version, at doi:10.1016/j.jcis.2009.04.096.

References

[1] V. Jacques, J.F. Desreus, in: Contast Agents I, vol. 221, 2002, pp. 123–164.
[2] R.B. Clarkson, in: Contast Agents I, vol. 221, 2002, pp. 123–164.
[3] M. Woods, E.W.C. Donald, A.D. Sherry, Chem. Soc. Rev. 35 (6) (2006) 500–511.
[4] R. Weissleder, K. Kelly, E.Y. Sun, T. Shtatland, L. Josephson, Nat. Biotechnol. 23 (11) (2005) 1418–1423.
[5] M.R. Caplan, E.V. Rosca, Ann. Biomed. Eng. 33 (8) (2005) 1113–1124.
[6] M.-C. Daniel, D. Astruc, Chem. Rev. 104 (1) (2004) 293–346.
[7] M. Brust, C.J. Kiely, Colloids Surf. A 202 (2–3) (2002) 175–186.
[8] A. Ulman, Chem. Rev. 96 (4) (1996) 1533–1554.
[9] W.R. Glomm, J. Disper. Sci. Technol. 26 (3) (2005) 389–414.
[10] M.J. Hostetler, R.W. Murray, Curr. Opin. Colloid Interface Sci. 2 (1) (1997) 42–50.
[11] D.J. Lavrich, S.M. Wetterer, S.L. Bernasek, G. Scoles, J. Phys. Chem. B 102 (18) (1998) 3456–3465.
[12] D.B. Pedersen, S. Duncan, J. Phys. Chem. A 109 (49) (2005) 11172–11179.
[13] S.J. Green, J.J. Pietron, J.J. Stokes, M.J. Hostetler, H. Vu, W.P. Wuelfing, R.W. Murray, Langmuir 14 (19) (1998) 5612–5619.
[14] O. Kohlmann, W.E. Steinmetz, X.-A. Mao, W.P. Wuelfing, A.C. Templeton, R.W. Murray, C.S. Johnson Jr., J. Phys. Chem. B 105 (37) (2001) 8801–8809.
[15] G.F. Paciotti, L. Tamarkin, Functionalized colloidal metal compositions for drug delivery. U.S. Patent 34542005072893, Jan. 28, 2005.
[16] L. Tamarkin, G.F. Paciotti Colloidal metal compositions and methods for drug targeting. U.S. Patent 137532002087509, April 30, 2002.
[17] R.K. Visaria, R.J. Griffin, B.W. Williams, E.S. Ebbini, G.F. Paciotti, C.W. Song, J.C. Bischof, Mol. Cancer Ther. 5 (4) (2006) 1014–1020.
[18] G.F. Paciotti, L. Myer, D. Weinreich, D. Goia, N. Pavel, R.E. McLaughlin, L. Tamarkin, Drug Deliv. 11 (3) (2004) 169–183.
[19] P.J. Debouttière, S. Roux, F. Vocanson, C. Billotey, O. Beuf, A. Favre-Reguillon, Y. Lin, S. Pellet-Rostaing, R. Lamartine, P. Perriat, O. Tillement, Adv. Funct. Mater. 16 (18) (2006) 2330–2339.
[20] C. Alric, J. Taleb, G. Le Duc, C. Mandon, C. Billotey, A. Le Meur-Herland, T. Brochard, F. Vocanson, M. Janier, P. Perriat, S. Roux, O. Tillement, J. Am. Chem. Soc. 130 (18) (2008) 5908–5915.
[21] J.-A. Park, P.A.N. Reddy, H.-K. Kim, I.-S. Kim, G.-C. Kim, Y. Chang, T.-J. Kim, Bioorg. Med. Chem. Lett. 18 (23) (2008) 6135–6137.
[22] A.M. Mohs, X.H. Wang, K.C. Goodrich, Y.D. Zong, D.L. Parker, Z.R. Lu, Bioconjug. Chem. 15 (6) (2004) 1424–1430.
[23] Y.D. Zong, X.H. Wang, K.C. Goodrich, A.M. Mohs, D.L. Parker, Z.R. Lu, Magn. Reson. Med. 53 (4) (2005) 835–842.
[24] Y.J. Fu, S. Laurent, R.N. Muller, Eur. J. Org. Chem. (23) (2002) 3966–3973.
[25] M.S. Konings, W.C. Dow, D.B. Love, K.N. Raymond, S.C. Quay, S.M. Rocklage, Inorg. Chem. 29 (8) (1990) 488–1491.
[26] T.H. Joo, K. Kim, M.S. Kim, Chem. Phys. Lett. 112 (1) (1984) 65–68.
[27] A.D. Sherry, W.P. Cacheris, K.T. Kuan, Magn. Reson. Med. 8 (2) (1988) 180–190.
[28] S.M. Baldwin, M.E. Kastner, Acta Crystallogr., Sect. C: Cryst. Struct. Commun. 58 (2002) M611–M612.
[29] W.J. Li, R.J. Wang, S.F. Si, Y.D. Li, J. Mol. Struct. 694 (1–3) (2004) 27–31.
[30] L.C. Yu, Z.F. Chen, Y.C. Liu, H. Liang, C.S. Zhou, Y. Zhang, J. Coord. Chem. 59 (11) (2006) 1203–1211.
[31] L. Michaelis, M.P. Schubert, J. Biol. Chem. 106 (1934) 331–341.
[32] A.E. Martell, R.M. Smith (Eds.), Critical Stability Constants, vol. 1, in: Amino Acids, 1974, p. 469.
[33] R.C. Major, X.Y. Zhu, J. Am. Chem. Soc. 125 (28) (2003) 8454–8455.
[34] C.F.G.C. Geraldes, A.M. Urbano, M.A. Hoefnagel, J.A. Peters, Inorg. Chem. 32 (11) (1993) 2426–2432.
[35] H. Lammers, F. Maton, D. Pubanz, M.W. vanLaren, H. vanBekkum, A.E. Merbach, R.N. Muller, J.A. Peters, Inorg. Chem. 36 (12) (1997) 2527–2538.
[36] H. Lammers, A.M. van der Heijden, H. van Bekkum, C.F.G.C. Geraldes, J.A. Peters, Inorg. Chim. Acta 268 (2) (1998) 249–255.
[37] J.A. Peters, Inorg. Chem. 27 (26) (1988) 4686–4691.
[38] S.-G. Lee, Magn. Reson. Chem. 38 (2000) 820–822.
[39] S. Aime, A. Barge, J.I. Bruce, M. Botta, J.A.K. Howard, J.M. Moloney, D. Parker, A.S. de Sousa, M. Woods, J. Am. Chem. Soc. 121 (24) (1999) 5762–5771.
[40] G.R. Choppin, P.A. Baisden, S.A. Khan, Inorg. Chem. 18 (5) (1979) 1330–1332.
[41] R.H. Terrill, T.A. Postlethwaite, C.H. Chen, C.D. Poon, A. Terzis, A.D. Chen, J.E. Hutchison, M.R. Clark, G. Wignall, J.D. Londono, R. Superfine, M. Falvo, C.S. Johnson, E.T. Samulski, R.W. Murray, J. Am. Chem. Soc. 117 (50) (1995) 12537–12548.
[42] C.Y. Jing, Y. Fang, Chem. Phys. 332 (1) (2007) 27–32.
[43] Z.J. Liu, G.Z. Wu, Spectrochim. Acta A 64 (1) (2006) 251–254.
[44] S. Panigrahi, S. Praharaj, S. Basu, S.K. Ghosh, S. Jana, S. Pande, T. Vo-Dinh, H. Jiang, T. Pal, J. Phys. Chem. B 110 (27) (2006) 13436–13444.
[45] S. Mandal, A. Gole, N. Lala, R. Gonnade, V. Ganvir, M. Sastry, Langmuir 17 (20) (2001) 6262–6268.
[46] M. Sastry, K.S. Mayya, K. Bandyopadhyay, Colloids Surf. A 127 (1–3) (1997) 221–228.
[47] P. Mulvaney, Langmuir 12 (3) (1996) 788–800.
[48] G.M. Dougherty, K.A. Rose, J.B.H. Tok, S.S. Pannu, F.Y.S. Chuang, M.Y. Sha, G. Chakarova, S.G. Penn, Electrophoresis 29 (5) (2008) 1131–1139.
[49] A. Aukrust, A. Raknes, C.E. Sjogren, L.K. Sydnes, Acta Chem. Scand. 51 (9) (1997) 918–926.
[50] Y.H. Kim, D.K. Lee, Y.S. Kang, Colloids Surf. A 257–258 (2005) 273–276.
[51] X.Q. Zou, H.F. Bao, H.W. Guo, L. Zhang, Q. Li, J.G. Jiang, L. Niu, S.J. Dong, J. Colloid Interface Sci. 295 (2) (2006) 401–408.
[52] M.R. Branham, A.D. Douglas, A.J. Mills, J.B. Tracy, P.S. White, R.W. Murray, Langmuir 22 (26) (2006) 11376–11383.
[53] M.J. Hostetler, J.E. Wingate, C.J. Zhong, J.E. Harris, R.W. Vachet, M.R. Clark, J.D. Londono, S.J. Green, J.J. Stokes, G.D. Wignall, G.L. Glish, M.D. Porter, N.D. Evans, R.W. Murray, Langmuir 14 (1) (1998) 7–30.
[54] S.W. Chen, R.W. Murray, Langmuir 15 (3) (1999) 682–689.
[55] B.S. Day, J.R. Morris, J. Chem. Phys. 122 (23) (2005).
[56] N. Yang, K. Aoki, J. Phys. Chem. B 109 (50) (2005) 23911–23917.
[57] N.J. Yang, K. Aoki, H. Nagasawa, J. Phys. Chem. B 108 (39) (2004) 15027–15032.
[58] B. Cage, S.E. Russek, R. Shoemaker, A.J. Barker, C. Stoldt, V. Ramachandaran, N.S. Dalal, Polyhedron 26 (12) (2007) 2413–2419.
[59] E. Nakamura, K. Makino, T. Okano, T. Yamamoto, M. Yokoyama, J. Control. Release 114 (3) (2006) 325–333.
[60] G.Y. Sun, J.H. Feng, F.Y. Jing, F.K. Pei, M.L. Liu, J. Magn. Magn. Mater. 265 (2) (2003) 123–129.
[61] M. Vaccaro, A. Accardo, G. D'Errico, K. Schillen, A. Radulescu, D. Tesauro, G. Morelli, L. Paduano, Biophys. J. 93 (5) (2007) 1736–1746.
[62] C.H. Cho, J. Urquidi, S. Singh, G.W. Robinson, J. Phys. Chem. B 103 (11) (1999) 1991–1994.

[63] N. Bloembergen, E.M. Purcell, R.V. Pound, Phys. Rev. 73 (1948) 679–712.
[64] R.B. Lauffer, Chem. Rev. 87 (5) (1987) 901–927.
[65] H.S. Choi, W. Liu, P. Misra, E. Tanaka, J.P. Zimmer, B.I. Ipe, M.G. Bawendi, J.V. Frangioni, Nat. Biotechnol. 25 (10) (2007) 1165–1170.
[66] V. Biju, T. Itoh, A. Anas, A. Sujith, M. Ishikawa, Anal. Bioanal. Chem. 391 (7) (2008) 2469–2495.
[67] S. Laurent, L.V. Elst, R.N. Muller, Contrast Med. Mol. Imag. 1 (3) (2006) 128–137.